Forward Electron Emission in Grazing Ion-Surface Collisions

E. A. Sánchez, O. Grizzi, M. L. Martiarena, and V. H. Ponce

Centro Atómico Bariloche, Comisión Nacional de Energía Atómica, 8400 San Carlos de Bariloche,
Río Negro, Argentina

(Received 3 November 1992; revised manuscript received 23 April 1993)

Electrons measured around the direction of specular reflection for 15–100 keV H^+, H_2^+, and He^+ scattering from single crystals show a strong dependence of their energy distribution with the surface topography. The maximum of the distribution appears at the convoy electron energy for rough surfaces and shifted to higher energies for smooth surfaces. This energy shift is visible for all the projectiles at 15 keV and increases with ion energy. The results are discussed in terms of transfer to the continuum of the ion Coulomb potential screened by the ion and electron surface induced charge.

PACS numbers: 79.20.Nc, 79.20.Rf

The electron emission produced in grazing ion-surface collisions carries information about the atomic, electronic, and magnetic structure of the topmost layer of the solid. There are two regions of electron observation angle of major interest: near the surface normal [1], and around the direction of the ion specular reflection. The present measurements are performed around the latter.

The main conclusions from previous measurements of electrons emitted from single crystals around the direction of specular reflection of the ions can be summarized as follows: (1) For H^+ projectiles of 20 keV to 1 MeV the electron energy spectra have a dominating peak centered at $E_{ce} = \frac{m}{M} E_p$, where m and M are the electron and projectile masses and E_p the ion energy. This peak is usually assigned to convoy electrons (CE) of the scattered projectiles [2–4]; its shape depends strongly on projectile energy, incidence angle, and electron observation angle [5]. (2) For atomic [6] (except H^+) and molecular [7] projectiles of energies higher than 250 keV/amu, the electron distribution shows a main structure centered at an energy $E_m > E_{ce}$. This structure is maximum at an electron observation angle several degrees larger than the angle for specular reflection of the ions. The energy difference $E_m - E_{ce}$ decreases with increasing projectile energy, is proportional to the projectile charge [6–8], and depends on the atomic number of both the target [9] and the projectile [6–8]. This new structure has been attributed to CE accelerated by the surface dynamic image potential induced by the projectile [3,6–12]. (3) Very recently, Koyama et al. [8] have measured electron energy spectra in 0.98 MeV/amu Xe^{27+} ions scattering from Al having simultaneously both structures, a narrow peak at E_{ce} and a broad structure centered at $E_m > E_{ce}$.

The aim of this work is to study (1) the electron energy spectra obtained by grazing bombardment of crystalline surfaces with H^+, H_2^+, and He^+ at low projectile energies, i.e., close to the threshold for formation of the dynamic image potential, and (2) the dependence of the electron energy spectra with the surface topography.

The experiments were performed in a UHV chamber that has been described previously [13]. The mass-analyzed ion beam is generated in a radio-frequency source, accelerated to 15–100 keV, and collimated to a spot size of ϕ, 0.5 mm diameter with angular divergence of $\approx 0.1°$. The targets were highly polished Si and Cu single crystals cleaned by repeated cycles of grazing sputtering with 700 eV Ar^+ and annealing until Auger electron spectroscopy showed no peaks due to contaminants. The surface topography of the samples was characterized by scanning electron microscopy (SEM), low energy electron diffraction (LEED), and measurements of the angular distributions of the reflected projectiles. The electrons were angular and energy analyzed by a custom made rotatable cylindrical mirror analyzer [13] working at 1% energy resolution and 0.7° angular resolution.

In order to produce different surface topographies in one target, 5 × 25 mm of Si(100) was annealed unevenly by placing a heating filament close to one end of the sample. With this procedure, the annealing temperature varied from ≈ 1400 K in the hottest end to 800 K in the coldest end of the sample. A study performed with SEM showed a high degree of roughness close to the end annealed at 1400 K and a smooth, structureless SEM image at the other end of the sample. The electron energy spectra obtained from different regions of the sample bombarded with 60 keV H^+ ions are shown in Fig. 1. Spectrum *a* comes from the sample region annealed at ≈ 1400 K. In this spectrum, the maximum appears centered at E_{ce}, in good agreement with the spectra measured previously in other samples [2, 4, 5]. By moving the sample in order to expose smoother regions to the ion beam, while keeping all the other experimental parameters constant, we have obtained the series of spectra *a* through *e*, where *e* comes from the sample region annealed at ≈ 900 K. Contrary to previous expectations [2–5], it can be seen from this series that while the CE peak decreases, another structure grows at an energy of ≈ 15 eV higher than E_{ce}. To our knowledge, this is the first time that this structure is seen with H^+ ions.

The same behavior was observed in a broad H^+ energy range (15–100 keV) for Cu(100) and Si(111) samples. Two 4 × 6 mm Si(111) samples were subjected to
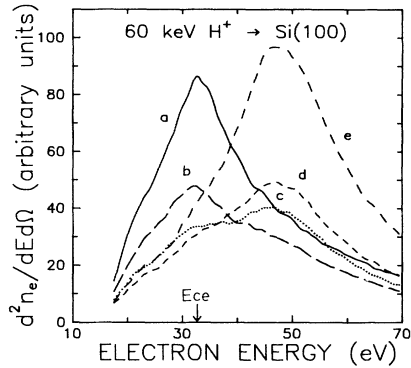
FIG. 1. Electron energy distributions for 60 keV H^+ bombardment of an unevenly annealed Si(100) sample. The incidence angle is $1°$ and the observation along the direction of the ion specular reflection. Spectra a to e come from sample regions annealed from 1400 K (spectrum a) to 900 K (e).

FIG. 2. Energy distributions of electrons ejected during 21 keV H^+ bombardment of two Si(111) samples prepared with different procedures (see text). The photographs show the corresponding surface images as seen with SEM.

different preparation procedures. One of them was prepared by many cycles of grazing sputtering and uniform annealing at 900 K (sample a), and the other by annealing at 1400 K (sample b). Sample a had a structureless SEM image and a sharp LEED pattern, while the SEM image of sample b showed a high degree of roughness with deep and big holes of ≈ 1 μm (see Fig. 2), and a LEED pattern with broader spots. The width of the angular distribution of the ions reflected from sample a was $1.3°$, that is 1.5 times narrower and twice as intense as that from sample b. The electron energy distributions coming from both samples bombarded by 21 keV H^+ ions are shown in Fig. 2. The distribution coming from the smooth surface has a shoulder at E_{ce} and a structure at $E_m > E_{ce}$, while a broad CE peak [2, 4, 5] dominates the spectrum coming from the rough surface. It can be seen in Fig. 2 that the CE appears accompanied by a higher secondary electron background, which is indicative of a stronger interaction between projectile and surface.

The electron energy spectra seen in Fig. 2 have different behaviors with the electron observation angle Θ. The intensity of the CE peak (spectrum b) is maximum at Θ slightly higher than the specular reflection of the projectiles, i.e., maximum at $\Theta = 1.2°$ for an incidence angle $\alpha = 0.8°$, while the maximum intensity of spectrum a occurs, for the same α, at $\Theta \geq 8°$. We cannot measure the exact position of this maximum since our electron analyzer rotates in a large circle which moves away from the scattering plane for large observation angles [13].

Once a relatively smooth surface has been obtained, the increase of the incidence angle to values where the projectiles start to penetrate the solid ($\alpha \gtrsim 2°$) still produces spectra similar to a of Fig. 2, though somewhat broader and with a smaller shoulder at E_{ce}.

The changes observed in the shape and position of the maximum of the electron energy and angular distributions are related to large modifications of the surface topography, and not to single atom steps or
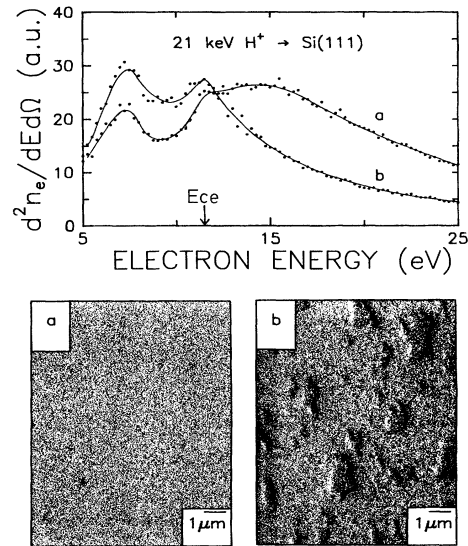
adatoms. Smooth surfaces modified by large doses (> 10^{16} ions/cm^2) of heavy ion bombardment (10 keV Ar^+ ions at large incident angles) or by evaporation of thick layers of Al or Au (> 400 Å) yield energy spectra with a main peak centered at E_{ce}. On the other hand, Ar^+ bombardment of smooth surfaces at energies lower than 1 keV with doses of about 10^{16} ions/cm^2, even though it is sufficient to blur the Si(111) reconstructed LEED pattern, still produces electron energy spectra with the maximum at energies higher than E_{ce}. Highly polished Si sufaces yield shifted electron structures even before any cleaning cycle was performed. At present, we cannot experimentally determine the minimum surface damage necessary to produce a CE peak. Nevertheless, since atomic scale roughness seems not to affect the shifted structure, and every time that roughness was detectable with the SEM (1000 Å), a CE peak was observed, we believe that the appearance of CE peaks is associated with roughness of the order of several tens to few hundred Å.

The results for H_2^+ and He^+ projectiles are similar to those described above for H^+, even for a projectile energy of 4 keV/amu, which is well within the regime of adiabatic response of surface electrons.

In order to compare our results for smooth surfaces to those measured previously in SnTe [7], we plot in Fig. 3(a) the ratio E_m/E_{ce} versus the projectile energy. The fact that smooth lines are sufficient to connect both sets of experimental points suggests that the same phenomenon affects the electron emission in the whole projectile energy range. Figure 3(b) shows the same experimental points plotted as $E_m - E_{ce}$ versus the projectile energy. Like in previous measurements at high projec-
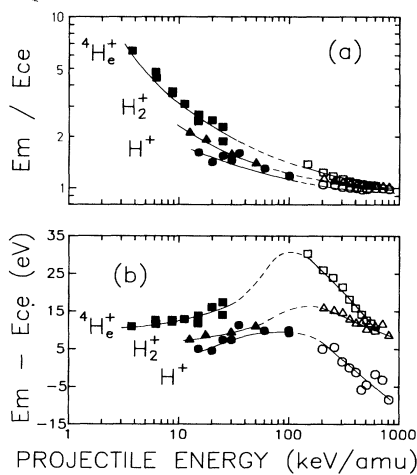
FIG. 3. (a) Ratio between the energies corresponding to the maximum of the electron energy distribution E_m and the calculated convoy electron energy E_{ce} as a function of projectile energy. Closed symbols, our measurements for a smooth Si(111) sample; open symbols, from Ref. [7] on SnTe. (b) Same experimental data plotted as $E_m - E_{ce}$ vs projectile energy. The lines were drawn to guide the eye.

FIG. 4. (a) (—): Effective potential energy φ_{eff}; (—·—): direct ion potential V_c; (— —): electron self-energy $-\frac{1}{2}V_e$ [15]; and ($\cdots$): ion induced potential energy $-V_Q$ [15] vs the coordinate z normal to the surface. The calculations were performed at $Z = 1.5$ a.u. for 60 keV H$^+$ colliding with a Si surface at $\alpha = 1°$. (b) Same as (a) along the specular direction of the reflected ion.

tile energy, $E_m - E_{ce}$ increases with projectile atomic number [9], but contrary to them, $E_m - E_{ce}$ increases with projectile energy, revealing a maximum around 100 keV/amu.

In the following we present a qualitative interpretation of the main features of the experiment, including the effect of surface roughness, and point out analogies and differences with previous theoretical models applied to smooth surfaces and higher projectile energy.

(a) The origin of outgoing ions: Projectiles moving close to the direction of specular reflection may originate on a surface region free from imperfections; they may also have undergone collisions with atoms placed at the steps and other structures of the surface, or even penetrate in the solid and still emerge close to this direction. Since the ion angular distributions are not as narrow as those obtained for particularly flat surfaces [14], our experimental situation may correspond to a combination of these cases.

(b) The potential energy for final electron states: During the interaction of the ion with surface atoms and electrons, there are continuum states centered on the projectile. Figure 4 shows the effective potential energy in which these electrons move

$$\varphi_{\mathrm{eff}}(\mathbf{R}, \mathbf{r}) = -Q/|\mathbf{r} - \mathbf{R}| + \varphi_{\mathrm{ind}}(\mathbf{R}, \mathbf{r}) , \qquad (1)$$

due to the direct ion potential and the contribution of the surface induced potentials

$$\varphi_{\mathrm{ind}}(\mathbf{R}, \mathbf{r}) = -V_Q(\mathbf{R}, \mathbf{r}) - \frac{1}{2}V_e(\mathbf{r}) . \qquad (2)$$

$\mathbf{R}$ and $\mathbf{r}$ are the ion and electron coordinates referred to the surface, respectively. This interaction produces,
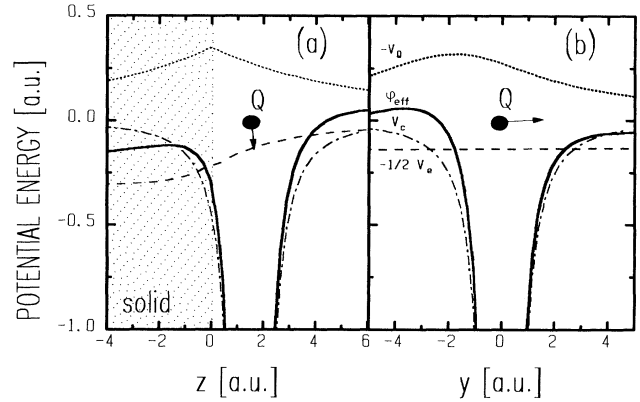
even for a proton, a positive contribution around the ion that decays slowly towards the vacuum region. For a projectile charge $Q > 1$, the ion-induced potential V_Q will prevail over the electron self-energy $-\frac{1}{2}V_e$ and will generate a potential barrier between ion and surface.

(c) Electron states: $\varphi_{\mathrm{eff}}(\mathbf{R}(t), \mathbf{r})$ has a weak dependence on time given by the ion velocity normal to the surface v_{nQ}. Electron transfer states form an outgoing wave packet initially centered on the ion; the evolution of each continuum orbital will be determined by the relation between the characteristic electron-ion velocity v_e' and v_{nQ}. When $v_e' > v_{nQ}$, the electron flies away, leaving behind the dipole charge distribution $-Q/|\mathbf{r} - \mathbf{R}| - V_Q \approx -2QZz/r^3$, where $Z = \mathbf{R} \cdot \hat{n}$, $z = \mathbf{r} \cdot \hat{n}$. The density of states at the continuum threshold is finite for partial waves with $l + 1/2 > \sqrt{2QZ}$, so the divergence typical of the Coulomb field is strongly weakened or disappears in this case [4].

The continuum levels ranging from the threshold value $E = 0$ (Fig. 4) may, in principle, be populated during the collision; those with $v_e' \leq v_{nQ}$ will remain close to the ion while the potential weakens. They will evolve nonadiabatically in the time-dependent potential $\varphi_{\mathrm{eff}}(\mathbf{R}(t), \mathbf{r})$ feeling a stronger attraction to the ion as the screening φ_{ind} dies away. The net effect will be a depopulation of these continuum states with transitions to low energy levels, including bound states. This cascading to lower energy levels is consistent with Monte Carlo calculations [11] where around 40% of the initial population of continuum levels ends up in bound states.

We expect that the asymptotic electron distribution will be depleted in the energy range from zero to a value of the order of $\varphi_{\mathrm{ind}}(\mathbf{R}, \mathbf{R})$. This effect will be enhanced in the case of highly charged ions, where the presence of the barrier in φ_{ind} between ion and surface will decrease

the electron transfer probability to low-lying continuum levels. Therefore, the asymptotic electron distribution will present a maximum shifted to energies $E_m > E_{ce}$; to determine the precise value of E_m will require a detailed evaluation of the nonadiabaticity in the post collision electron evolution, which we will present in a future publication. Finally, outgoing electrons will experience the focusing effect of the induced potential φ_{ind}, which has a gradient that defines the induced electric field ϵ_{ind}. This will produce an anisotropy in the electron distribution, shifting its maximum towards the direction of ϵ_{ind}.

(d) The influence of surface topography: The idea of the outgoing electron evolution relies on the presence of a weak time dependence of $\varphi_{ind}(\mathbf{R}(t), \mathbf{r})$. This requires a smooth surface, with a roughness that does not produce large and persistent changes in the value of the ion-surface distance Z. A different situation appears when the mean time dependence of $Z \approx v_{nQ}t$ is strongly changed, for example, by imperfections in the form of down-steps of several lattice parameters of depth, that extend long enough for the electron to be far away from the surface before they come to an end. In this case Z increases suddenly as the electron recedes from the surface, $\varphi_{ind}(\mathbf{R}(t), \mathbf{r})$ becomes negligible and the Coulombic ion-electron potential characterizes the postcollision evolution. This explains our observation of a CE peak for surfaces with imperfections observable with SEM.

(e) Analogies and differences with the convoy electron acceleration model (CEAM) [3, 6, 10–12]: The CEAM assumes an initial electron state that is at the threshold of the Coulomb potential of the ion [11]; afterwards, the induced potential is turned on, so the energy level of the electron state is shifted by a value of the order of $\varphi_{ind}(\mathbf{R}, \mathbf{R})$. Here, the idea of the electron being accelerated by the induced electric field reflects the fact that the electron will gain in asymptotic kinetic energy what it received in potential energy when it was close to the ion in the initial stages of the time evolution. Measured values for H, He, Li, and C ions in 6 mrad grazing collisions on SnTe show a peak for the electron distribution at 100 mrad that goes from 165 eV (H) to 250 eV (C); the isotachic value is 163 eV for a 0.3 MeV/amu projectile. The induced potential can be approximated by $\varphi_{ind} = (Q - 1/2)\pi w_s/2v_Q$ close to the ion [15]; using the measured effective charges for Q, the energy of the peaks result in 187, 227, 242, and 275 eV for H, He, Li, and C, respectively. These results are not far off the measurements and previous Monte Carlo calculations [11], pointing to the equivalence between our image of the electron evolving with the potential energy φ_{eff}, and the CEAM view of the electron accelerated by ϵ_{ind}.

The main difference between these two descriptions arises from those continuum states between the threshold of φ_{eff} and the value $\varphi_{ind}(\mathbf{R}, \mathbf{R})$, that are not considered in the CEAM. As pointed out in (c) these states may be populated at small ion-surface separations, but due to the postcollision interaction they will be depopulated through transitions to low energy and bound states. In this way, the electron distribution will show a maximum for a value $E_m > E_{ce}$.

We summarize our results as follows: The energy and angular distribution of the electrons ejected around the direction of specular reflection for H^+, H_2^+, and He^+ scattering from single crystals depends strongly on the surface topography. For rough surfaces, the maximum intensity of the energy and angular distributions is at the calculated CE energy and close to the angle of ion specular reflection, respectively. For smooth surfaces, this maximum is shifted to higher electron energies and to higher observation angles. Contrary to measurements at high energy, for smooth surfaces this energy shift increases with projectile energy and becomes maximum at ≈ 100 keV/amu. The sample preparation method and the projectile energy range used in our experiment allowed us to observe this behavior for H^+, and for He^+ in the regime of adiabatic response of surface electrons. A model based on transfer to the continuum of the screened ion potential describes qualitatively the experimental results for both types of surface topographies.

[1] C. Rau, K. Waters, and N. Chen, Phys. Rev. Lett. **64**, 1441 (1990).

[2] L. F. de Ferrariis and R. A. Baragiola, Phys. Rev. A **33**, 4449 (1986).

[3] M. Hasegawa, K. Kimura, and M. Mannami, J. Phys. Soc. Jpn. **57**, 1834 (1988); M. Hasegawa et al., Nucl. Instrum. Methods Phys. Res., Sect. B **53**, 285 (1991).

[4] H. Winter, P. Strohmeier, and J. Burgdörfer, Phys. Rev. A **39**, 3895 (1989).

[5] E. A. Sánchez, M. L. Martiarena, O. Grizzi, and V. H. Ponce, Phys. Rev. A **45**, R1299 (1992).

[6] A. Koyama, Nucl. Instrum. Methods Phys. Res., Sect. B **67**, 103 (1992).

[7] Y. Mizuno et al., Nucl. Instrum. Methods Phys. Res., Sect. B **67**, 164 (1992).

[8] A. Koyama et al., Phys. Rev. Lett. **65**, 3156 (1990).

[9] H. Ishikawa et al., Nucl. Instrum. Methods Phys. Res., Sect. B **67**, 160 (1992).

[10] T. Iitaka et al., Phys. Rev. Lett. **65**, 3160 (1990).

[11] K. Kimura, M. Tsuji, and M. Mannami, Phys. Rev. A **46**, 2618 (1992).

[12] J. Burgdörfer, Nucl. Instrum. Methods Phys. Res., Sect. B **24/25**, 139 (1987); **67**, 1 (1992).

[13] L. F. de Ferrariis, F. Tutzauer, E. A. Sánchez, and R. A. Baragiola, Nucl. Instrum. Methods Phys. Res., Sect. A **281**, 43 (1989).

[14] H. Winter, Comments At. Mol. Phys. **26**, 287 (1991).

[15] F. J. García de Abajo and P. M. Echenique, Phys. Rev. B **46**, 2663 (1992).
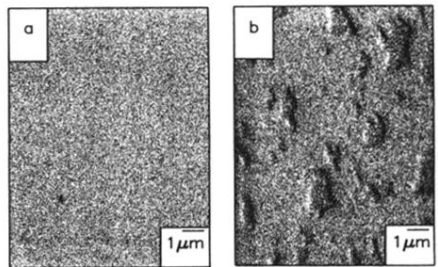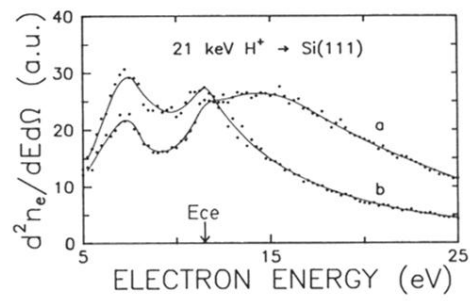
FIG. 2. Energy distributions of electrons ejected during 21 keV H$^+$ bombardment of two Si(111) samples prepared with different procedures (see text). The photographs show the corresponding surface images as seen with SEM.